DOI: 10.1002/cbic.201100709

# Stereoselective Hydride Transfer by Aryl-Alcohol Oxidase, a Member of the GMC Superfamily

Aitor Hernández-Ortega,[a] Patricia Ferreira,[b] Pedro Merino,[c] Milagros Medina,[b] Victor Guallar,[d] and Angel T. Martínez*[a]

Primary alcohol oxidation by aryl-alcohol oxidase (AAO), a flavoenzyme providing $H_2O_2$ to ligninolytic peroxidases, is produced by concerted proton and hydride transfers, as shown by substrate and solvent kinetic isotope effects (KIEs). Interestingly, when the reaction was investigated with synthesized (*R*)- and (*S*)-α-deuterated *p*-methoxybenzyl alcohol, a primary KIE (≈6) was observed only for the *R* enantiomer, revealing that the hydride transfer is highly stereoselective. Docking of *p*-methoxybenzyl alcohol at the buried crystal active site, together with QM/MM calculations, showed that this stereoselectivity is due to the position of the hydride- and proton-receiving atoms (flavin N5 and His502 Nε, respectively) relative to the alcohol Cα-substituents, and to the concerted nature of transfer (the pro-*S* orientation corresponding to a 6 kcal mol$^{-1}$ penalty with respect to the pro-*R* orientation). The role of His502 is supported by the lower activity (by three orders of magnitude) of the H502A variant. The above stereoselectivity was also observed, although activities were much lower, in AAO reactions with secondary aryl alcohols (over 98% excess of the *R* enantiomer after treatment of racemic 1-(*p*-methoxyphenyl)ethanol, as shown by chiral HPLC) and especially with use of the F501A variant. This variant has an enlarged active site that allow better accommodation of the α-substituents, resulting in higher stereoselectivity (*S*/*R* ratios) than is seen with AAO. High enantioselectivity in a member of the GMC oxidoreductase superfamily is reported for the first time, and shows the potential for engineering of AAO for deracemization purposes.

## Introduction

Aryl-alcohol oxidase (AAO, EC 1.1.3.7) is a secreted flavooxidase involved in the extracellular degradation of lignin by some white-rot basidiomycetes (including *Pleurotus* and *Bjerkandera* species) through provision of the $H_2O_2$ required by ligninolytic peroxidases.[1] Removal of the recalcitrant lignin polymer is the key step for carbon recycling in land ecosystems and is also a central issue for the industrial use of renewable plant biomass in the sustainable production of chemicals, materials, and fuels.[2,3]

The reducing power for $O_2$ activation to $H_2O_2$ comes from aromatic alcohols that AAO oxidizes to the corresponding aldehydes, with *p*-methoxybenzyl alcohol being one of the preferred reducing substrates of *Pleurotus eryngii* AAO.[4] This enzyme also oxidizes some aromatic aldehydes to acids, acting on their *gem*-diol forms.[5] In this and related white-rot fungi, a continuous supply of $H_2O_2$ for lignin degradation is available through the redox-cycling of secreted *p*-methoxybenzaldehyde (*p*-anisaldehyde), the main extracellular aromatic metabolite of *Pleurotus*, in a process involving intracellular aromatic dehydrogenases together with AAO.[6,7]

To be a good AAO substrate, an alcohol must have a primary hydroxy group conjugated with a planar double bond system (benzylic, β-naphthylmethyl, and aliphatic polyunsaturated alcohols[8] are all included) establishing a stacking interaction with an active-site tyrosine.[9] Substrate oxidation by other members of the glucose/methanol/choline oxidase (GMC) superfamily, a large group of oxidoreductases including well-known flavoenzymes (such as glucose oxidase, choline oxidase, and cholesterol oxidase, among others) has been investigated. The consensus mechanism involves substrate activation by a catalytic base and oxidation of the resulting alkoxide to the aldehyde (and eventually to the acid in a second step) by the FAD cofactor (N5 atom), which is then reoxidized by $O_2$.[10]

Stereoselective (or stereospecific) redox reactions have been described in oxidases, dehydrogenases, and other oxidoreductases, often being associated with active site architectures.[11–17]

[a] *A. Hernández-Ortega,[+] A. T. Martínez*
*Centro de Investigaciones Biológicas (CIB)*
*Consejo Superior de Investigaciones Científicas (CSIC)*
*Ramiro de Maeztu 9, 28040 Madrid (Spain)*
*E-mail: ATMartinez@cib.csic.es*

[b] *P. Ferreira,[+] M. Medina*
*Department of Biochemistry and Molecular and Cellular Biology and*
*Institute of Biocomputation and Physics of Complex Systems*
*University of Zaragoza*
*50009 Zaragoza (Spain)*

[c] *P. Merino*
*Department of Organic Chemistry and*
*Instituto de Síntesis Química y Catálisis Homogénea (ISQCH)*
*CSIC, University of Zaragoza*
*50009 Zaragoza (Spain)*

[d] *V. Guallar*
*ICREA Joint BSC-IRB research programme in Computational Biology*
*Barcelona Supercomputing Center*
*Jordi Girona 29, 08034 Barcelona (Spain)*

[+] *These authors contributed equally to this work.*

*Supporting information for this article is available on the WWW under http://dx.doi.org/10.1002/cbic.201100709.*

  

Microbial and, more recently, enzymatic transformations are being actively investigated for a variety of asymmetric redox reactions of increasing commercial interest.[18] These include drug synthesis, because more than half of all drug candidates include chiral centers.[19] Although hydrolases are more frequently used in chiral synthesis, oxidoreductases are also valuable tools for the production of compounds of industrial interest by asymmetric transformations.[18] In these reactions, both enantioselective synthesis and resolution of chiral mixtures are possible by use of different oxidoreductases.

**Table 1.** Steady state and transient state kinetic constants for alcohol (Al) and $O_2$ (Ox) in AAO oxidation of α-deuterated and normal (α-protiated) *p*-methoxybenzyl alcohol (the latter in $H_2O$ or $^2H_2O$ buffer).[a]

| | Deuterated alcohol (in $H_2O$) | | | Normal alcohol | |
|---|---|---|---|---|---|
| | (*R*)-[α-$^2$H] | (*S*)-[α-$^2$H] | [α-$^2H_2$] | $H_2O$ | $^2H_2O$ |
| Steady state | | | | | |
| $k_{cat}$ | 38 ± 1 | 144 ± 2 | 25 ± 1 | 196 ± 2 | 131 ± 1 |
| $K_{m(Al)}$ | 34 ± 1 | 45 ± 1 | 25 ± 1 | 49 ± 1 | 38 ± 1 |
| $k_{cat}/K_{m(Al)}$ | 1110 ± 17 | 3190 ± 101 | 1020 ± 16 | 3980 ± 113 | 2510 ± 103 |
| $K_{m(Ox)}$ | 47 ± 1 | 134 ± 5 | 32 ± 1 | 159 ± 5 | 114 ± 4 |
| $k_{cat}/K_{m(Ox)}$ | 808 ± 18 | 1070 ± 38 | 785 ± 20 | 1236 ± 38 | 1150 ± 38 |
| Transient state | | | | | |
| $k_{red}$ | 25 ± 1 | 77 ± 1 | 12 ± 1 | 139 ± 16 | 79 ± 2 |
| $K_d$ | 36 ± 2 | 33 ± 1 | 23 ± 6 | 26 ± 6 | 23 ± 3 |

[a] Maximum steady state constants [catalytic constant ($k_{cat}$, $s^{-1}$), Michaelis–Menten constant ($K_m$, μM), and efficiency ($k_{cat}/K_m$, $s^{-1}$ mM$^{-1}$)] were estimated in bisubstrate kinetics at 25 °C, with use of Equations (1) and (2). Transient kinetic constants [including reduction constant ($k_{red}$, $s^{-1}$) and alcohol dissociation constant ($K_d$, μM)] were estimated at 12 °C, with use of Equation (3) (means ± S.D.s).

In this study, α-monodeuterated—*R* and *S* enantiomers—and α-dideuterated *p*-methoxybenzyl alcohol derivatives were synthesized and evaluated as AAO substrates. Substrate and solvent kinetic isotope effects (KIEs), modeling of *p*-methoxybenzyl alcohol docking at the active site of the crystal structure, and QM/MM calculations were used to gain information on the mechanism of primary aromatic alcohol oxidation by AAO, revealing that hydride abstraction stereoselectively affects only one of the two α-hydrogens. The obtained conclusions were extended to chiral aromatic alcohols, the stereoselective oxidation of which was enhanced by site-directed mutagenesis, resulting in an AAO variant with an enlarged active site.

## Results

### AAO oxidation of α-deuterated *p*-methoxybenzyl alcohol

α-Monodeuterated and α,α -dideuterated *p*-methoxybenzyl alcohol derivatives were synthesized (by use of different deuterated reducing agents) to confirm that primary alcohol oxidation by AAO involves Cα hydride transfer and to investigate the possible stereoselectivity of this reaction. The *R* and *S* monodeuterated isomers were obtained with 96% enantiomeric excesses (*ees*) and showed identical physical and spectroscopic properties with the exception of the signs of optical rotation (the $^1$H NMR spectra of the mono- and dideuterated alcohols are shown in Figure S1 in the Supporting Information).

The steady state constants for the normal (α-protiated) and different α-deuterated—(*R*)-[α-$^2$H], (*S*)-[α-$^2$H], and [α-$^2H_2$]—*p*-methoxybenzyl alcohols were calculated by simultaneously varying the concentrations of alcohol and $O_2$ (in bisubstrate kinetics) to obtain maximum values by extrapolating to saturation conditions. Michaelis–Menten constants ($K_m$) and efficiencies ($k_{cat}/K_m$) for both alcohol (Al) and oxygen (Ox) are provided in Table 1, together with the global catalytic constants ($k_{cat}$). The AAO transient state reduction ($k_{red}$) and dissociation ($K_d$) constants, estimated under anaerobic conditions by stopped-flow spectrophotometry, are also provided in Table 1.

The KIE values on the apparent steady state kinetic constants for the three α-deuterated alcohols were estimated at five $O_2$ concentrations (0.051, 0.128, 0.273, 0.566, and 1.279 mM; Table S1). The $^Dk_{cat(app)}$ values for the (*R*)-[α-$^2$H]-*p*-methoxybenzyl and [α-$^2H_2$]-*p*-methoxybenzyl alcohols increased significantly with the concentration of $O_2$, whereas their $^D(k_{cat(app)}/K_{m(Al)(app)})$ values were significant but similar for the different $O_2$ concentrations, and the KIE values for (*S*)-[α-$^2$H]-*p*-methoxybenzyl alcohol were always near unity (Figure 1). From the above results, the steady state KIE values (Table 2) were calculated as the ratios between the values of the kinetic constants for the protiated and the three α-deuterated alcohols, in the bisubstrate kinetics.

The differences in the observed rates of AAO reduction by the protiated and deuterated alcohol substrates, as well as their concentration dependence, could be also observed by anaerobic stopped-flow spectrophotometry (Figure 2). The

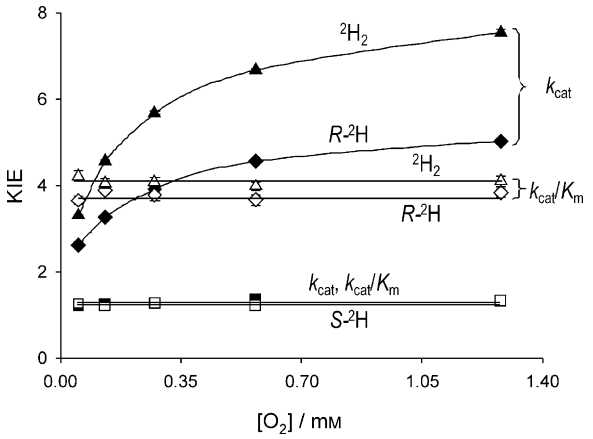


**Figure 1.** Influence of $O_2$ concentration on steady state KIE values. The KIEs on apparent kinetic constants ($k_{cat}$ and $k_{cat}/K_m$) for α-monodeuterated [(*R*)-$^2$H and (*S*)-$^2$H], and α-dideuterated ($^2H_2$) *p*-methoxybenzyl alcohol oxidation by AAO were estimated at five $O_2$ concentrations (assays at 25 °C, and data fitted to Equation (4)).

  

**Table 2.** Substrate (*p*-methoxybenzyl alcohol) and solvent KIE values on AAO steady state constants.[a]

| | $k_{cat}$ | $K_{m(Al)}$ | $k_{cat}/K_{m(Al)}$ | $K_{m(Ox)}$ | $k_{cat}/K_{m(Ox)}$ |
|---|---|---|---|---|---|
| (*R*)-[α-$^2$H] | 5.2 ± 0.1 | 1.4 ± 0 | 3.6 ± 0.1 | 3.4 ± 0.1 | 1.5 ± 0.1 |
| (*S*)-[α-$^2$H] | 1.4 ± 0 | 1.1 ± 0 | 1.2 ± 0.1 | 1.2 ± 0.1 | 1.2 ± 0.1 |
| [α-$^2$H$_2$] | 7.9 ± 0.1 | 2.0 ± 0.1 | 3.9 ± 0.1 | 5.0 ± 0.2 | 1.6 ± 0.1 |
| $^2H_2O$ | 1.5 ± 0 | 1.3 ± 0.1 | 1.6 ± 0.1 | 1.4 ± 0.1 | 1.1 ± 0.1 |

[a] The KIE values are the ratios between maximum activities (from bisubstrate kinetics) on α-protiated/α-deuterated alcohols and in $H_2O/^2H_2O$ buffer (means ± S.D.s).

strongest rate decreases, with respect to the protiated *p*-methoxybenzyl alcohol, were observed for the *R* enantiomer and the dideuterated alcohol, but some decrease was also observed for the *S* enantiomer. From these data, the values of the KIEs on the AAO reduction kinetic constants ($^Dk_{red}$ and $^DK_d$) were obtained (Table 3).

The AAO turnover ($k_{cat}$) and reduction ($k_{red}$) rates of the deuterated substrates showed significant KIEs for (*R*)-[α-$^2$H]-*p*-methoxybenzyl alcohol, close to those obtained for the α-dideuterated alcohol, whereas the KIEs for the (*S*)-[α-$^2$H]-*p*-methoxybenzyl alcohol were very much lower. The KIE values for the alcohol catalytic efficiency—$^D(k_{cat}/K_{m(Al)})$—were slightly lower than the $^Dk_{cat}$ values, revealing that substrate binding is only slightly affected by the isotopic substitutions, in agreement with the low values of $K_d$ KIE. The above primary values for the KIEs on AAO turnover indicate that the breakdown of the alcohol (*R*)-Cα-$^1$H/$^2$H bond is limiting the rate of flavin reduction and, therefore, of the overall catalysis. They also show that the pro-*R* hydrogen (i.e., the hydrogen, the substitution of which would provide the *R* enantiomer) is the one involved in the hydride transfer reaction to the flavin.

The small but significant $k_{cat}$ and $k_{red}$ KIEs for (*S*)-[α-$^2$H]-*p*-methoxybenzyl alcohol, together with the KIEs found for [α-$^2$H$_2$]-*p*-methoxybenzyl alcohol, which are higher than found for the *R* isomer, indicate α-secondary KIEs. The multiple KIEs for primary and secondary KIEs were especially evident under transient state conditions, under which the $^Dk_{red}$ value for [α-$^2$H$_2$]-*p*-methoxybenzyl alcohol was close to the product of those for the *R* and *S* isomers.

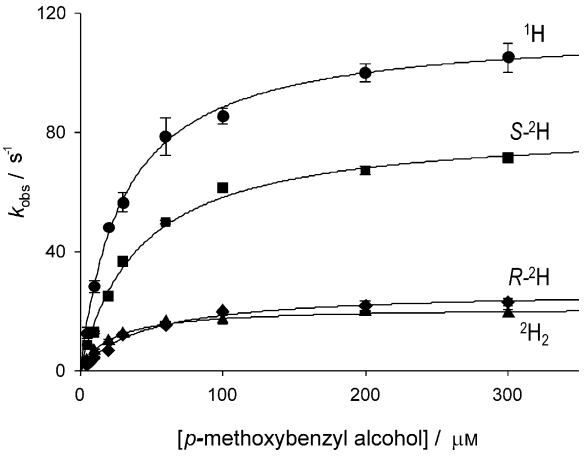


**Figure 2.** Dependence of rates of AAO reduction on concentrations of protiated and deuterated substrates. The effect of α-protiated ($^1$H), α-monodeuterated [(*R*)-$^2$H and (*S*)-$^2$H], and α-dideuterated ($^2H_2$) *p*-methoxybenzyl alcohol concentration on the transient state observed rates for AAO reduction were estimated (assays at 12 °C by anaerobic stopped-flow spectrophotometry and data were fitted to Equation (3)).

**Table 3.** Substrate (*p*-methoxybenzyl alcohol) and solvent values of KIEs on AAO transient state constants.[a]

| | $k_{red}$ | $K_d$ | | $k_{red}$ | $K_d$ |
|---|---|---|---|---|---|
| (*R*)-[α-$^2$H] | 6.5 ± 0.1 | 1.5 ± 0.4 | (*S*)-[α-$^2$H] | 1.5 ± 0.1 | 1.2 ± 0.3 |
| [α-$^2$H$_2$] | 9.3 ± 0.1 | 1.1 ± 0.4 | $^2H_2O$ | 1.4 ± 0.1 | 1.1 ± 0.3 |

[a] Transient state KIE values were calculated by fitting data to Equation (5) (means ± S.D.s).

### Solvent KIEs in alcohol oxidation by AAO

Oxidation of *p*-methoxybenzyl alcohol by AAO was also studied in deuterated buffer to confirm the timing of kinetic steps involving solvent-exchangeable protons (including the alcohol hydroxy proton), in the context of the hydride transfer described above. The maximum KIE values for steady state reactions in deuterated buffer, estimated as the ratios between the maximum constants from bisubstrate kinetics in $H_2O$ and $^2H_2O$, are included in Table 2, and the transient state solvent KIE values showing the effect of deuterated buffer on the enzyme reduction constants are provided in Table 3.

Although the KIE values for solvent were much lower than for substrate, low but consistent solvent KIEs were observed for AAO $k_{cat}$ and $k_{red}$, and a slightly higher value was obtained for the alcohol catalytic efficiency, whereas the solvent KIE on $K_d$ was close to unity. The solvent effect is confirmed by a multiple transient state KIE ($^{D,D_2O}k_{red}$, 13.5 ± 0.9, from comparison of AAO reduction by α-protiated alcohol in $H_2O$ and by α-dideuterated alcohol in $^2H_2O$) being similar to the product of the substrate and solvent $k_{red}$ KIE values. Multiple KIEs were not investigated in bisubstrate steady state reactions, but could be observed for apparent kinetic constants in air-saturated $^2H_2O$ reactions, with $^Dk_{cat(app)}$ (7.0 ± 0.4) and $^D(k_{cat(app)}/K_{m(Al)(app)})$ (6.1 ± 0.6) values being equal to or higher than the products of the substrate and solvent KIEs for $k_{cat(app)}$ (5.4 ± 0.1 and 1.3 ± 0.1, respectively) and $k_{cat(app)}/K_{m(Al)(app)}$ (3.7 ± 0.3 and 1.2 ± 0.1, respectively) under these reaction conditions.

Because $^2H_2O$ increases the viscosity of the medium (affecting diffusion-limited steps) *p*-methoxybenzyl alcohol oxidation was evaluated at a 30% glycerol concentration (resulting in medium viscosity similar to $^2H_2O$ reactions). No significant effect on bisubstrate $k_{cat}$ (0.99 ± 0.01), $k_{cat}/K_{m(Al)}$ (1.03 ± 0.04), or $k_{cat}/K_{m(Ox)}$ (1.01 ± 0.04) was observed, confirming that the observed KIEs are due to the effect of solvent-exchangeable protons on the AAO reaction, and not to the increase in viscosity.

  

### QM/MM calculations for docked *p*-methoxybenzyl alcohol

The AAO crystal structure [Protein Data Bank (PDB), entry 3FIM] reveals a buried active site with direct connection to the solvent blocked by the side chains of Tyr92, Phe397, and Phe501. In a recent study,[9] PELE (protein energy landscape exploration), a state-of-the-art protein–ligand induced fit modeling software package, was used to elucidate the access of *p*-methoxybenzyl alcohol to the AAO active site. The final position of the *p*-methoxybenzyl alcohol is illustrated in Figure 3A

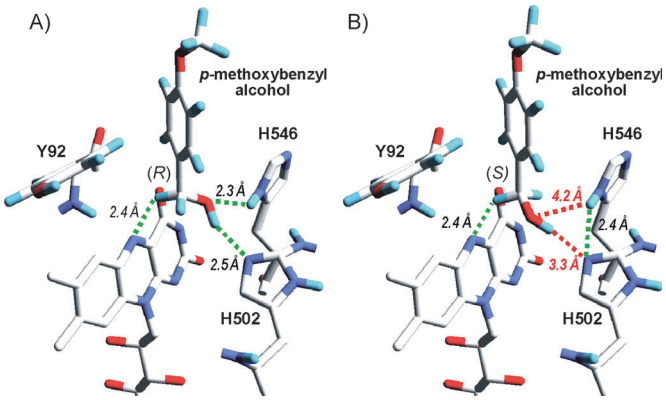


**Figure 3.** Docking of *p*-methoxybenzyl alcohol at the AAO active site (lateral view of flavin). A) At the position provided by PELE, the pro-*R* and hydroxy hydrogens are at transfer distance from the flavin N5 and the unprotonated Nε of His502, respectively (green lines). Moreover, the protonated Nδ of His546 forms a hydrogen bond to the hydroxy group (green line). B) However, when a pro-*S* hydride transfer position was tried, the hydroxy group was too far (red lines) from His502 and His546, and a new H-bond appears between the histidines (green line). Based on PDB ID: 3FIM. As Corey–Pauling–Koltun (CPK) colored sticks.

and has similar distances (≈2.5 Å) between its hydroxy hydrogen and His502 Nε and between its pro-*R* Cα-hydrogen and the flavin N5. The protonated Nδ of His546 is also close to the hydroxy group, and an edge-to-plane stacking interaction between the *p*-methoxybenzyl alcohol and Tyr92 aromatic rings is produced as previously described[9] (a stereoview of *p*-methoxybenzyl alcohol docking is provided in Figure S2).

With the aim of confirming the AAO preference for hydride abstraction from the pro-*R* position, we performed a QM/MM energy scan for the rotation of the dihedral between the phenyl ring and the C1-Cα-OH plane, as shown on comparison of Figure 3A and 3B. The energy scan is based on several geometry optimizations with constrained values for the dihedral angles. The three main players in the hydrogen bond pattern—the substrate, His502, and His546—were included in the quantum region. The scan, involving six optimized intermediate points along the dihedral rotation, resulted in a 6 kcal $mol^{-1}$ penalty for the pro-*S* orientation, with a 10 kcal $mol^{-1}$ rotation energy barrier. In this case (pro-*S* oxidation) larger distances would exist between the substrate hydroxy group and the His502 and His546 side chains, which would form a new H-bond, preventing their contribution to catalysis (Figure 3B).

### Reactions with secondary aromatic alcohols

Figure 4A shows a flavin *si*-side view of *p*-methoxybenzyl alcohol docked at the AAO active site (also including Phe501, His502, and His546). Although the Phe501 side chain points towards its benzylic position, the *p*-methoxybenzyl alcohol can

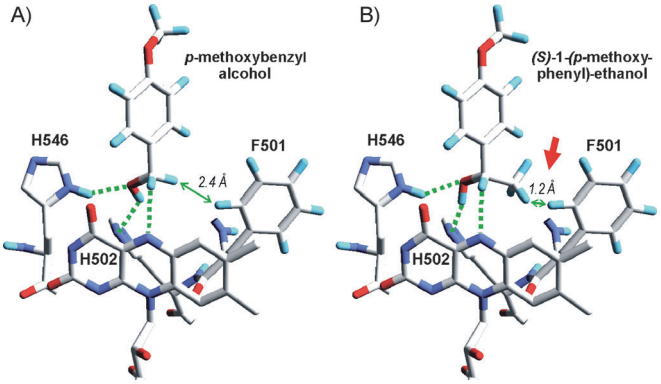


**Figure 4.** Docking of primary and of secondary aromatic alcohols at the AAO active site (view from flavin *si*-side). In contrast with the situation observed in A) for *p*-methoxybenzyl alcohol, when (*S*)-1-(*p*-methoxyphenyl)ethanol is positioned in the same catalytically relevant position, in B) steric hindrance prevents accommodation of the α-methyl group due to collision (red arrow) with the Phe501 side chain. Based on PDB ID: 3FIM. As CPK colored sticks.

easily adopt the catalytically relevant position described above (with the hydroxy group and the pro-*R* Cα hydrogens at transfer distances from the flavin N5 and the His502 Nε, respectively). However, if the pro-*S* hydrogen is simply substituted by a methyl group—in 1-(*p*-methoxyphenyl)ethanol—steric hindrance (red arrow in Figure 4B) is produced when the substrate is forced to adopt a position compatible with catalysis.

The above predictions were confirmed by experimental data showing a value for AAO apparent efficiency in oxidizing 1-(*p*-methoxyphenyl)ethanol, estimated from $H_2O_2$ release (at 25 °C under air saturation), of only $3.59\times10^{-3}$ $s^{-1}$ $mM^{-1}$ (in comparison with 4070 $s^{-1}$ $mM^{-1}$ for *p*-methoxybenzyl alcohol under the same conditions) with a $k_{cat(app)}$ value of only 0.179 $s^{-1}$ (cf. 120 $s^{-1}$ for *p*-methoxybenzyl alcohol). However, when an F501A variant was obtained, and its activities on secondary alcohols (relative to *p*-methoxybenzyl alcohol activity) were compared with those of native (wild-type) AAO (Table 4) it could be observed that removal of the Phe501 side chain (hindering AAO accommodation of secondary alcohols) resulted in a 60-fold higher relative activity with 1-(*p*-methoxyphenyl)ethanol and a 19-fold higher activity with (*S*)-1-(*p*-fluorophenyl)ethanol.

Interestingly, during the slow oxidation (of the order of 0.1 $s^{-1}$ $M^{-1}$) of 1-(*p*-fluorophenyl)ethanol by native AAO and, especially, by the F501A variant, a net preference for the *S* enantiomer was observed (Figure 5A and 5C) as revealed by the formation of *p*-fluoroacetophenone shown in the difference spectra (Figure 5B and 5D).

In the case of racemic 1-(*p*-methoxyphenyl)ethanol, the stereoselectivity of the reaction was confirmed by chiral HPLC, which showed only one major peak after the AAO treatment

  

**Table 4.** AAO and F501A oxidation of secondary 1-(*p*-methoxyphenyl)ethanol and *R* and *S* enantiomers of 1-(*p*-fluorophenyl)ethanol relative to primary *p*-methoxybenzyl alcohol activity ($\times 10^{-6}$) and stereoselectivity ratio.[a]

| | Native AAO | F501A variant |
|---|---|---|
| 1-(*p*-methoxyphenyl)ethanol (racemic) | 53 | 3130 |
| (*R*)-1-(*p*-fluorophenyl)ethanol | 0.043 | 0.263 |
| (*S*)-1-(*p*-fluorophenyl)ethanol | 0.914 | 17.37 |
| stereoselectivity *S*/*R* ratio | 21 | 66 |

[a] Linear oxidation of secondary alcohols (1 mM) to the corresponding ketones was followed spectrophotometrically during long-term incubation in air-saturated (0.273 mM $O_2$ concentration) phosphate (pH 6, 0.1 M) at 25 °C, and $k_{obs}$ values are relative to those obtained for *p*-methoxybenzyl alcohol oxidation by native AAO (120 $s^{-1}$ $mM^{-1}$) and F501A ($3.8\times 10^{-3}$ $s^{-1}$ $mM^{-1}$) under the same conditions.

(Figure 6) with an *ee* > 98%. The absolute configuration of the remaining enantiomer was ascertained by measuring the sign of the optical rotation, which proved to be positive, corresponding to the *R* isomer,[20,21] thus confirming that the enzyme had selectively oxidized the *S* isomer. This highly stereoselective oxidation implies abstraction of the *R* hydrogen, as described above for the primary alcohols.

More importantly, the AAO preference for (*S*)-1-(*p*-fluorophenyl)ethanol was increased threefold when the bulky side chain of Phe501 was removed in the F501A variant, which shows a stereoselectivity *S*/*R* ratio of 66:1 for this secondary alcohol (Table 4). This is consistent with the higher relative rates of oxidation of 1-(*p*-methoxyphenyl)ethanol and (*S*)-1-(*p*-fluorophenyl)ethanol by the F501A variant mentioned above (relative to native AAO) due to better accommodation of secondary alcohols at the active site of the engineered variant.

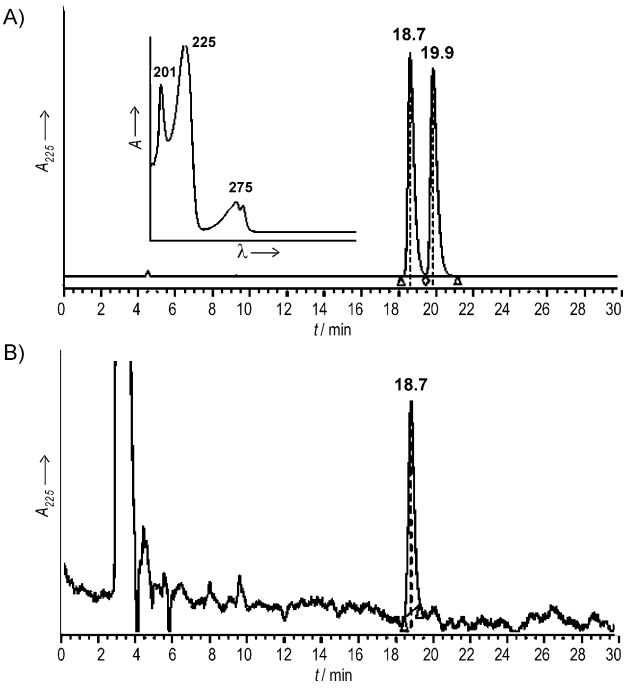


**Figure 6.** Chiral HPLC analysis confirming deracemization of 1-(*p*-methoxyphenyl)ethanol by AAO. A) Control chromatogram of the racemic mixture, showing two peaks corresponding to the *S* and *R* enantiomers. B) Chromatogram after its treatment with AAO, resulting in enzymatic deracemization yielding the *R* enantiomer (as shown by its optical rotation) with high *ee* (> 98%). The analyses were performed with a Chiralcel IB column, and peaks were monitored at 225 nm. The UV spectrum corresponding to the 1-(*p*-methoxyphenyl)ethanol peaks is included in the inset.

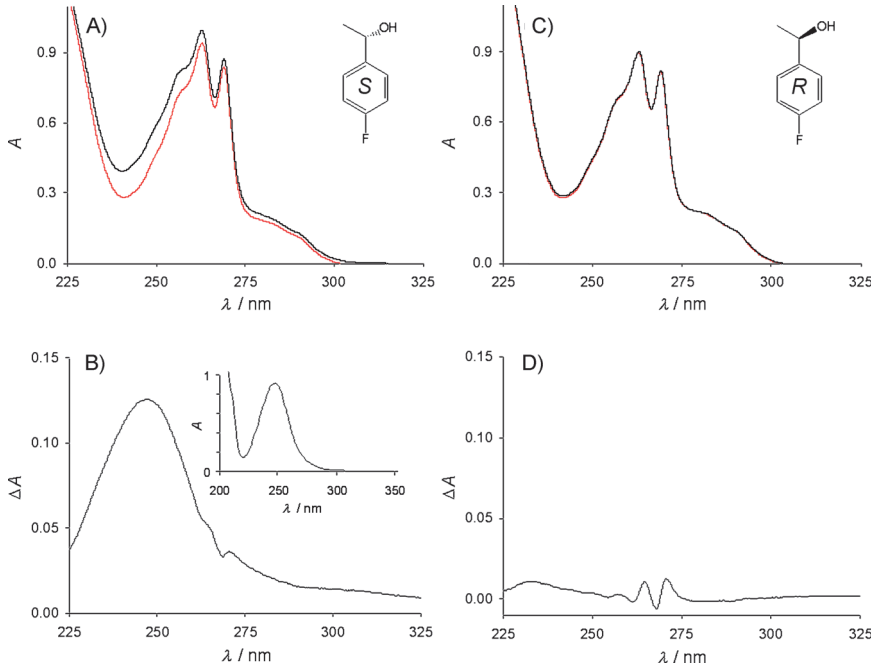


**Figure 5.** Incubation of alcohol *S* and *R* enantiomers with the F501A variant. Initial (red) and final (black) UV spectra were obtained during 20 h incubation of A) (*S*)-(*p*-fluorophenyl)ethanol and C) (*R*)-(*p*-fluorophenyl)ethanol (both 1 mM) at 25 °C in phosphate (pH 6, 0.1 M) containing F501A (1.7 μM). B) Difference spectra showed the *p*-fluoroacetophenone maximum only for the *S* enantiomer. The UV spectrum of authentic *p*-fluoroacetophenone is also shown (inset).

## Discussion

### Oxidation mechanism by AAO, a GMC oxidoreductase

The primary substrate KIEs on AAO maximum steady state constants (from bisubstrate kinetics) and transient state constants for α-dideuterated *p*-methoxybenzyl alcohol (≈8–9 $k_{cat}/k_{red}$ KIE) indicate that this flavooxidase abstracts one of the Cα hydrogens (together with the two electrons) during substrate oxidation. Hydride transfer, to cofactor flavin N5, is nowadays the consensus mechanism for substrate oxidation in the GMC oxidoreductase super-

  

family,[10] and the substrate KIE values obtained here are of the same order as those reported for the model GMC choline oxidase.[22,23] However, the KIE on the apparent efficiency of AAO was independent of oxygen concentration, suggesting irreversible hydride transfer in AAO, in contrast with what has been reported for choline oxidase, with which the $^{D}(k_{cat(app)}/K_{m(app)})$ values increase with oxygen concentration.[24]

Moreover, the low but consistent solvent KIE values ($\approx$1.5) found on both AAO steady state (from bisubstrate kinetics) and transient state constants are indicative of hydride transfer to flavin being concerted with transfer of a solvent-exchangeable proton (in a partially limiting reaction). The same tendencies had been reported previously when the effects of substrate and solvent deuteration on apparent kinetic constants were measured from air reactions (instead of from bisubstrate kinetic).[25] The multiple KIE found (from comparison of reactions of $\alpha$-protiated alcohol in $H_2O$ and reactions of $\alpha$-dideuterated alcohol in $^2H_2O$) confirms that the observed solvent effect is due to the abstraction of the substrate hydroxy proton by a catalytic base being concerted with hydride abstraction by the flavin. The very strong decreases in both $k_{cat}$ and $k_{red}$ in the H502A variant (2890- and 1830-fold, respectively),[9] together with its position at the active site, strongly suggest that His502 is the catalytic base. A concerted transfer mechanism has also been reported for AAO oxidation of some aromatic aldehydes through their *gem*-diol species.[5]

In this respect, AAO differs from the related choline oxidase[23] and other members of the GMC oxidoreductase superfamily, in which nonconcerted (stepwise) hydride and proton transfer (resulting in a stable alkoxide intermediate) has been proposed as a general mechanism.[10] More recently, a nonconcerted transfer mechanism to flavin and His548 (homologous to AAO His502) has been reported in pyranose 2-oxidase.[26,27] In AAO, recent QM/MM calculations found that proton transfer precedes hydride transfer in alcohol oxidation, but no stable intermediate is produced, so the two reactions are therefore considered asynchronous concerted transfers.[9] AAO is not an exception among flavoenzymes, because a highly concerted transfer mechanism takes place in D-amino acid oxidase, the paradigm of flavin enzymes.[28] Moreover, in choline oxidase and some flavoproteins exhibiting similar catalysis (such as flavocytochrome $b_2$), changes from nonconcerted to concerted mechanisms have been obtained by mutagenesis of residues involved in abstraction of the hydroxy proton, as revealed by low solvent and multiple KIEs,[29–31] similar to those reported here for native AAO. Finally, small but significant solvent KIEs have also been detected during the low-efficiency oxidation of benzylic alcohols by galactose oxidase,[14,32] the stereoselectivity of which is discussed below.

### Stereoselectivity on primary (and secondary) aryl alcohols

When the two enantiomers of monodeuterated *p*-methoxybenzyl alcohol—the (*S*)-[$\alpha$-$^2$H] and (*R*)-[$\alpha$-$^2$H] forms—were assayed as AAO substrates, primary KIE values of around 6 were obtained for the *R* enantiomer under both steady state and transient state conditions. This revealed for the first time that the AAO hydride abstraction from primary aryl alcohols, which are its natural substrates, is produced selectively from the pro-*R* position. Stereoselective (or stereospecific) substrate oxidation has been reported in some other oxidases, including the copper-radical enzyme galactose oxidase[14] and the flavoenzymes D-amino acid oxidase[33] and vanillyl-alcohol oxidase.[11] Moreover, glucose oxidase is selective, oxidizing the $\beta$-anomeric form of D-glucose.[34,35] However, as far as we know, this is the first time that stereoselective primary alcohol oxidation (with only one of the two $\alpha$-hydrogens involved in hydride abstraction) has been reported for a member of the GMC superfamily of oxidoreductases.

In addition to the above primary KIE, a significant $\alpha$-secondary substrate KIE ($\approx$1.4) was also observed in the AAO reactions, being indicative of hydrogen tunneling, as described for tyrosine hydroxylase.[36] In recent years, quantum tunneling for hydride transfer has been reported in many other oxidoreductases,[37,38] including related flavoproteins such as choline oxidase.[23,39,40] Secondary KIEs are often a consequence of a change in the hybridization state of the donor in proceeding from the reactants to the transition state. The multiple KIE values obtained suggest that this rehybridization is occurring at the same transition state as hydride transfer.

The AAO stereoselectivity in hydride abstraction from the pro-*R* C$\alpha$ position in primary aromatic alcohols revealed by deuterium labeling was also demonstrated by the use of secondary (chiral) aromatic alcohols as substrates, in spite of the low activities of the enzyme with these compounds. This was first revealed by the over 20-times faster oxidation of (*S*)-1-(*p*-fluorophenyl)ethanol, implying hydride abstraction from the *R* position, in relation to its *R* enantiomer. The selective removal of the *S* enantiomer of racemic 1-(*p*-methoxyphenyl)ethanol by AAO (resulting in an *ee* $>$98% in the remaining enantiomer) was then confirmed by chiral HPLC. AAO could therefore be used for deracemization of secondary alcohol mixtures for isolation of chiral aromatic alcohols. These include products of industrial interest for which microbial deracemization has already been considered.[41] The use of AAO for enzymatic deracemization would not require the introduction of stereoselectivity but the extension of its activity to secondary alcohols, as discussed below.

In stereoselective galactose oxidase, which oxidizes benzyl alcohol, although with much lower efficiency (0.36 $s^{-1}$ $mM^{-1}$) than it does 1-*O*-methyl-$\alpha$-D-galactopyranoside (29.50 $s^{-1}$ $mM^{-1}$),[14] directed evolution from an improved variant[42] has been performed to extend the activity to secondary aryl alcohols.[43] The unique mutation (K330M) introduced during evolution provides a more hydrophobic active site that might favor 1-phenylethanol binding. In AAO, PELE docking of *p*-methoxybenzyl alcohol at the crystal structure[44] found that the benzylic position is at the bottom of the active site cavity (with the primary hydroxy and pro-*R* hydrogens orientated as discussed above) and the rest of the cavity is occupied by the alcohol aromatic ring. Therefore, to accommodate secondary alcohols, the bottom part of the cavity should be enlarged. To conclude this study, engineering of the AAO active site was addressed by rational design, resulting in the F501A variant, in

  

which the bulky aromatic side chain of Phe501 (located in front of the pro-*S* hydrogen) was removed. As recently shown,[45] this mutation reduces the efficiency of the enzyme for oxidation of primary alcohols, but its relative activity with secondary alcohols is significantly improved. More importantly, when this variant was assayed on the *R* and *S* enantiomers of 1-(*p*-fluorophenyl)ethanol, its stereoselectivity was highly increased with respect to native AAO.

#### Structural bases for AAO catalysis and stereoselectivity

With use of the AAO crystal structure[44] as the starting point, the PELE software successfully simulated the migration of *p*-methoxybenzyl alcohol to the buried active site of AAO,[9] where it adopted a catalytically relevant position. Interestingly, at this position its pro-*R* α-hydrogen is at 2.4 Å from the flavin N5, enabling hydride transfer consistently with the substrate KIE results discussed above. Simultaneously, the hydroxy hydrogen is 2.5 Å from the His502 Nε, enabling its contribution as a base in accepting the proton for alcohol activation. An additional hydrogen bond to the substrate from His546, an important residue for catalysis, the removal of which reduced (≈40-fold) AAO activity and alcohol binding,[9] is also observed.

In contrast, if we try to place the *p*-methoxybenzyl alcohol with the pro-*S* α-hydrogen in a suitable position for hydride transfer to the flavin N5, the result is energetically unfavorable, as revealed by QM/MM calculations. The pro-*S* structure presents an overall rearrangement of the hydrogen bond pattern. The hydroxy group is too far from His502 and His546 to form strong hydrogen bonds and efficient catalysis. As a result there is a new intra-protein hydrogen bond between the two histidines. Therefore, the KIEs for the two α-monodeuterated *p*-methoxybenzyl enantiomers, as well as the small but stereoselective activity of AAO on chiral secondary aryl alcohols, are in agreement with the predicted position of the alcohol at the active site.

We postulate that the stereoselectivity in AAO is related to the active site architecture and reaction mechanism revealed by the KIE studies, which imply the asynchronous but concerted transfer of hydroxy proton (to His502) and Cα hydride (to flavin N5),[9] in contrast to the nonconcerted (stepwise) mechanism suggested as a consensus in GMC oxidoreductases.[10] In the concerted transfer catalyzed by AAO, once the alcohol substrate is accommodated with the hydroxy group pointing towards His502, as shown by PELE docking, only the pro-*R* hydrogen is facing the flavin N5, resulting in the high hydride abstraction selectivity, whereas in stepwise transfer mechanisms some conformational changes are possible.

## Conclusions

Using the synthesized deuterated enantiomers of the natural alcohol substrate of AAO, we have found, for the first time in a member of the GMC superfamily, highly stereoselective abstraction of one of the two primary alcohol hydrogens. The significant KIE previously observed for the α-dideuterated substrate was indicative of a hydride transfer oxidation mechanism. Moreover, our experimental results indicate, in agreement with theoretical analysis, that substrate activation by the catalytic base is concerted with hydride transfer, instead of the stepwise process suggested for GMC oxidoreductases. Modeling of the active site geometry revealed the atomic mechanism of stereoselectivity, involving alcohol hydrogen bonds to His502 and His546. The catalytically relevant modeled position also indicated the potential of the F501A variant for oxidation of secondary alcohols. The variant was produced and showed improved stereoselective activity with 1-phenylethanol derivatives. These results provide relevant information on the catalytic mechanisms in GMC oxidoreductases and at the same time show the potential for use of AAO or its engineered variants as industrial biocatalysts in the production of chiral aromatic alcohols of interest for the fine chemicals or pharmaceutical sectors.

## Experimental Section

**Chemicals**: *p*-Methoxybenzyl alcohol, *p*-fluorobenzyl alcohol, 1-(*p*-methoxyphenyl)ethanol (racemic), (*R*)-1-(*p*-fluorophenyl)ethanol, (*S*)-1-(*p*-fluorophenyl)ethanol, *p*-methoxybenzaldehyde, *p*-fluoroacetophenone, methyl *p*-methoxybenzoate, and the deuterated reducing agents used below were purchased from Sigma–Aldrich.

**Synthesis of deuterated substrates**: Dideuterated [α-$^2H_2$]-*p*-methoxybenzyl alcohol was prepared by reduction of methyl *p*-methoxybenzoate with $LiAl^2H_4$.[46] (*R*)-[α-$^2$H]-*p*-Methoxybenzyl alcohol was prepared from *p*-methoxybenzaldehyde,[47] with use of (*S*)-alpine borane in the enantioselective reduction of the intermediate deuterated aldehyde. The *S* enantiomer and the racemic mixture were prepared in the same way but with use of (*R*)- and racemic alpine borane, respectively. $^1$H NMR (400 MHz) and DEPT $^{13}$C NMR (100 MHz) spectra in $C^2HCl_3$ were used to confirm the products obtained.

**Native enzyme and mutated variant**: Native recombinant AAO from *P. eryngii* was obtained by *E. coli* expression of the mature AAO cDNA (GenBank AF064069) followed by in vitro activation for cofactor incorporation and correct folding.[48] The F501A variant was prepared by PCR with use of the QuikChange site-directed mutagenesis kit (Stratagene; the oligonucleotides used are described in the Supporting Information). The mutation was confirmed by sequencing (GS-FLX sequencer from Roche) and the variant was produced and refolded as for the native enzyme. Enzyme concentrations were determined with a Cary-100-Bio spectrophotometer and use of the molar absorbances of native AAO ($\varepsilon_{463}$ = 11 050 $M^{-1}cm^{-1}$) and its F501A variant ($\varepsilon_{463}$ = 10 389 $M^{-1}cm^{-1}$) estimated by heat denaturation.

**Steady-state and transient-state kinetics**: Oxidation of *p*-methoxybenzyl alcohol to *p*-methoxybenzaldehyde ($\varepsilon_{285}$ = 16 950 $M^{-1}cm^{-1}$) was followed spectrophotometrically (Cary-100-Bio). Maximum steady state constants were estimated in bisubstrate kinetics by varying both the alcohol and $O_2$ concentrations and extrapolating to saturation conditions. Transient-state kinetic measurements of enzyme reduction constants were performed by stopped-flow spectrophotometry (Applied Photophysics SX18.MV equipment) under anaerobic conditions. The experimental details and equations used for steady state and transient state data analyses are provided in the Supporting Information.

  

**KIEs in *p*-methoxybenzyl alcohol oxidation**: The effect of substrate α-deuteration—*R*, *S*, and dideuterated forms—on AAO reactions was estimated (in the pH-independent portion of the pH activity profile) under both steady state and transient state conditions, the former in bisubstrate kinetics to obtain maximum values. Solvent KIE values were also estimated in both steady state and transient state reactions with use of $^2H_2O$ buffer, and possible viscosity effects were considered (the experimental details and equations used for data analysis are provided in the Supporting Information).

**Secondary alcohol oxidation**: Oxidation of 1-(*p*-methoxyphenyl)-ethanol by native AAO and by its F501A variant was measured from the $H_2O_2$ generated, by means of an HRP-coupled assay with AmplexRed (Invitrogen) at 25 °C in air-saturated sodium phosphate (pH 6, 0.1 M). Assays were initiated by addition of AAO, and formation of the resofurin product was monitored ($\varepsilon_{585}$ 52 000 $M^{-1}cm^{-1}$).

Oxidation of (*R*)-1-(*p*-fluorophenyl)ethanol and (*S*)-1-(*p*-fluorophenyl)ethanol to *p*-fluoroacetophenone, the molar absorbance of which was determined here ($\varepsilon_{247}$ 11 616 $M^{-1}cm^{-1}$), was evaluated in air-saturated phosphate buffer (pH 6, 0.1 M) at 25 °C, after long-term incubation (up to 24 h), due to the very low AAO activity with this alcohol. For chiral HPLC (see below), long-term oxidation of racemic 1-(*p*-methoxyphenyl)ethanol (20 mM, 5–10 mg) with AAO (20 μM) was also assayed. After incubation in phosphate (pH 6, 50 mM) at 25 °C, the enzyme was removed by ultrafiltration and the sample was freeze-dried for analysis. Activities relative to *p*-methoxybenzyl alcohol (under the same conditions) were estimated for both secondary alcohols for purposes of comparison.

**Chiral HPLC and optical rotation**: The enantioselectivity of racemic 1-(*p*-methoxyphenyl)ethanol oxidation was quantified by HPLC (Waters Alliance), after salt removal from the sample, with use of a Chiralcel IB column (4.6×250 mm, 5 μm; Daicel Chemical Industries, Ltd.), elution with *n*-hexane/propan-2-ol (98:2, *v*/*v*) at 1.0 mL $min^{-1}$, and a diode-array detector (peak monitoring at 225 nm). Optical rotation was measured in chloroform with a Jasco polarimeter.

**QM/MM**: QM/MM calculations were performed with the Qsite program.[49] The DFT method with the M06 functional,[50] the ultrafine pseudospectral grid, and the 6–31G* basis set were applied for the QM/MM geometry optimization. The quantum region included the substrate, His502, and His546. The classical region used a conjugate gradient minimizer (with an rmsg of 0.01) and the OPLS-AA force field. Because of the large influence of the classical point charges on the wave function, the non-bonding cutoff was set to 100 Å and updated every 10 steps. In the scan optimization, all atoms within 20 Å of the substrate were allowed to move. The dihedral scan was built with six intermediate minimizations along the C1–Cα dihedral (maintaining the aromatic ring fixed). The initial structure (pro-*R*) was taken from our previous simulation,[9] based on migration of *p*-methoxybenzyl alcohol into the AAO crystal structure (3FIM).[44] In this previous study we performed an exhaustive analysis of the histidine protonation steps and an initial equilibration of the system and the explicit solvent. A PDB file with the initial coordinates for the simulation is available in the Supporting Information.

## Acknowledgements

*This work was supported by Spanish projects BIO2008-01533, BIO2011-26694 (to A.T.M. and co-workers), BIO2010-1493 (to M.M.), CTQ2010-19606 (to P.M.), and CTQ2010-18123 (to V.G.), and by PEROXICATS (KBBE-2010-4-265397; to A.T.M.) and PELE (ERC-2009-Adg 25027; to V.G.) European projects. The authors thank Jesús Jiménez-Barbero (CIB, Madrid) for his useful comments and suggestions, and the Barcelona Supercomputing Center for computational resources. A.H.-O. acknowledges a contract from the Comunidad de Madrid.*

**Keywords:** enantioselectivity · enzyme catalysis · flavooxidases · isotope effects · QM/MM

[1] F. J. Ruiz-Dueñas, Á. T. Martínez, *Microb. Biotechnol.* **2009**, *2*, 164 – 177.
[2] Á. T. Martínez, F. J. Ruiz-Dueñas, M. J. Martínez, J. C. del Río, A. Gutiérrez, *Curr. Opin. Biotechnol.* **2009**, *20*, 348 – 357.
[3] A. J. Ragauskas, C. K. Williams, B. H. Davison, G. Britovsek, J. Cairney, C. A. Eckert, W. J. Frederick, J. P. Hallett, D. J. Leak, C. L. Liotta, J. R. Mielenz, R. Murphy, R. Templer, T. Tschaplinski, *Science* **2006**, *311*, 484 – 489.
[4] F. Guillén, A. T. Martínez, M. J. Martínez, *Eur. J. Biochem.* **1992**, *209*, 603 – 611.
[5] P. Ferreira, A. Hernández-Ortega, B. Herguedas, J. Rencoret, A. Gutiérrez, M. J. Martínez, J. Jiménez-Barbero, M. Medina, A. T. Martínez, *Biochem. J.* **2010**, *425*, 585 – 593.
[6] F. Guillén, C. S. Evans, *Appl. Environ. Microbiol.* **1994**, *60*, 2811 – 2817.
[7] A. Gutiérrez, L. Caramelo, A. Prieto, M. J. Martínez, A. T. Martínez, *Appl. Environ. Microbiol.* **1994**, *60*, 1783 – 1788.
[8] M. Medina, P. Ferreira, F. Guillén, M. J. Martínez, W. J. H. van Berkel, Á. T. Martínez, *Biochem. J.* **2005**, *389*, 731 – 738.
[9] A. Hernández-Ortega, K. Borrelli, P. Ferreira, M. Medina, A. T. Martínez, V. Guallar, *Biochem. J.* **2011**, *436*, 341 – 350.
[10] G. Gadda, *Biochemistry* **2008**, *47*, 13745 – 13753.
[11] R. H. H. van den Heuvel, M. W. Fraaije, C. Laane, W. J. H. van Berkel, *J. Bacteriol.* **1998**, *180*, 5646 – 5651.
[12] H. L. Holland, H. K. Weber, *Curr. Opin. Biotechnol.* **2000**, *11*, 547 – 553.
[13] M. J. Knapp, K. Rickert, J. P. Klinman, *J. Am. Chem. Soc.* **2002**, *124*, 3865 – 3874.
[14] S. G. Minasian, M. M. Whittaker, J. W. Whittaker, *Biochemistry* **2004**, *43*, 13683 – 13693.
[15] M. A. Gilabert, L. G. Fenoll, F. Garcia-Molina, P. A. Garcia-Ruiz, J. Tudela, F. Garcia-Canovas, J. N. Rodríguez-López, *Biol. Chem.* **2004**, *385*, 1177 – 1184.
[16] S. Águila, R. Vázquez-Duhalt, R. Tinoco, M. Rivera, G. Pecchi, J. B. Alderete, *Green Chem.* **2008**, *10*, 647 – 653.
[17] B. Yuan, A. Page, C. P. Worrall, F. Escalettes, S. C. Willies, J. J. W. McDouall, N. J. Turner, J. Clayden, *Angew. Chem.* **2010**, *122*, 7164 – 7167; *Angew. Chem. Int. Ed.* **2010**, *49*, 7010 – 7013.
[18] T. Matsuda, R. Yamanaka, K. Nakamura, *Tetrahedron: Asymmetry* **2009**, *20*, 513 – 557.
[19] J. S. Carey, D. Laffan, C. Thomson, M. T. Williams, *Org. Biomol. Chem.* **2006**, *4*, 2337 – 2347.
[20] A. S. Y. Yim, M. Wills, *Tetrahedron* **2005**, *61*, 7994 – 8004.
[21] B. A. Barros-Filho, M. D. F. de Oliveira, T. L. G. Lemos, M. C. de Mattos, G. de Gonzalo, V. Gotor-Fernández, V. Gotor, *Tetrahedron: Asymmetry* **2009**, *20*, 1057 – 1061.
[22] G. Gadda, *Biochim. Biophys. Acta Proteins Proteomics* **2003**, *1650*, 4 – 9.
[23] F. Fan, G. Gadda, *J. Am. Chem. Soc.* **2005**, *127*, 2067 – 2074.
[24] F. Fan, G. Gadda, *J. Am. Chem. Soc.* **2005**, *127*, 17954 – 17961.
[25] P. Ferreira, A. Hernández-Ortega, B. Herguedas, A. T. Martínez, M. Medina, *J. Biol. Chem.* **2009**, *284*, 24840 – 24847.
[26] J. Sucharitakul, T. Wongnate, P. Chaiyen, *Biochemistry* **2010**, *49*, 3753 – 3765.
[27] T. Wongnate, J. Sucharitakul, P. Chaiyen, *ChemBioChem* **2011**, *12*, 2577 – 2586.
[28] L. Pollegioni, W. Blodig, S. Ghisla, *J. Biol. Chem.* **1997**, *272*, 4924 – 4934.
[29] P. Sobrado, P. F. Fitzpatrick, *Biochemistry* **2003**, *42*, 15208 – 15214.
[30] M. Ghanem, G. Gadda, *Biochemistry* **2005**, *44*, 893 – 904.
[31] K. Rungsrisuriyachai, G. Gadda, *Biochemistry* **2010**, *49*, 2483 – 2490.
[32] M. M. Whittaker, D. P. Ballou, J. W. Whittaker, *Biochemistry* **1998**, *37*, 8426 – 8436.

  

[33] A. Mattevi, M. A. Vanoni, F. Todone, M. Rizzi, A. Teplyakov, A. Coda, M. Bolognesi, B. Curti, *Proc. Natl. Acad. Sci. USA* **1996**, *93*, 7496 – 7501.
[34] D. Keilin, E. F. Hartree, *Biochem. J.* **1952**, *50*, 331 – 341.
[35] V. Leskovac, S. Trivic, G. Wohlfahrt, J. Kandrac, D. Pericin, *Int. J. Biochem. Cell Biol.* **2005**, *37*, 731 – 750.
[36] P. A. Frantom, R. Pongdee, G. A. Sulikowski, P. F. Fitzpatrick, *J. Am. Chem. Soc.* **2002**, *124*, 4202 – 4203.
[37] J. Pu, J. Gao, D. G. Truhlar, *Chem. Rev.* **2006**, *106*, 3140 – 3169.
[38] Z. D. Nagel, J. P. Klinman, *Nat. Chem. Biol.* **2009**, *5*, 543 – 550.
[39] M. J. Sutcliffe, L. Masgrau, A. Roujeinikova, L. O. Johannissen, P. Hothi, J. Basran, K. E. Ranaghan, A. J. Mulholland, D. Leys, N. S. Scrutton, *Phil. Trans. R. Soc. Lond. B* **2006**, *361*, 1375 – 1386.
[40] I. Lans, J. R. Peregrina, M. Medina, M. Garcia-Viloca, A. Gonzalez-Lafont, J. M. Lluch, *J. Phys. Chem. B* **2010**, *114*, 3368 – 3379.
[41] G. R. Allan, A. J. Carnell, *J. Org. Chem.* **2001**, *66*, 6495 – 6497.
[42] L. H. Sun, I. P. Petrounia, M. Yagasaki, G. Bandara, F. H. Arnold, *Protein Eng.* **2001**, *14*, 699 – 704.
[43] F. Escalettes, N. J. Turner, *ChemBioChem* **2008**, *9*, 857 – 860.
[44] I. S. Fernández, F. J. Ruiz-Dueñas, E. Santillana, P. Ferreira, M. J. Martínez, A. T. Martínez, A. Romero, *Acta Crystallogr. D* **2009**, *65*, 1196 – 1205.
[45] A. Hernández-Ortega, F. Lucas, P. Ferreira, M. Medina, V. Guallar, A. T. Martínez, *J. Biol. Chem.* **2011**, *286*, 41105 – 41114.
[46] M. Fetizon, Y. Henry, N. Moreau, G. Moreau, M. Golfier, T. Prange, *Tetrahedron* **1973**, *29*, 1011 – 1014.
[47] J. R. Walker, R. W. Curley, *Tetrahedron* **2001**, *57*, 6695 – 6701.
[48] F. J. Ruiz-Dueñas, P. Ferreira, M. J. Martínez, A. T. Martínez, *Protein Expression Purif.* **2006**, *45*, 191 – 199.
[49] Schrödinger Inc., *QSite 5.6*, LCC, New York, **2010**.
[50] Y. Zhao, D. G. Truhlar, *Theor. Chem. Acc.* **2008**, *120*, 215 – 241.

Received: November 11, 2011
Published online on January 23, 2012

  